Engineering non-antibody human proteins as efficient scaffolds for selective, receptor-targeted drug delivery.

Naroa Serna[1,2,3,§], Victor Pallarès[3,4,5,§], Ugutz Unzueta[2,3,4,5,*], Annabel Garcia-Leon[3,4,5], Eric Voltà-Durán[1,2,3], Alejandro Sánchez-Chardi[7,8], Eloi Parladé[1,2,3], Ariana Rueda[3,4,5] Isolda Casanova[3,4,5], Aïda Falgàs[3,4,5], Lorena Alba-Castellón[3,4,5], Jorge Sierra[6], Antonio Villaverde[1,2,3], Esther Vázquez[1,2,3,*] and Ramón Mangues[3,4,5].

[§] Equally contributed.

[*] Corresponding authors.

[1] Institut de Biotecnologia i de Biomedicina, Universitat Autònoma de Barcelona, Bellaterra, 08193 Barcelona, Spain.

[2] Departament de Genètica i de Microbiologia, Universitat Autònoma de Barcelona, Bellaterra, 08193 Barcelona, Spain.

[3] CIBER de Bioingeniería, Biomateriales y Nanomedicina (CIBER-BBN), Bellaterra, 08193 Barcelona, Spain.

[4] Biomedical Research Institute Sant Pau (IIB Sant Pau), Sant Antoni Mª Claret 167, 08025 Barcelona Spain.

[5] Josep Carreras Leukaemia Research Institute (IJC Campus Sant Pau), 08025 Barcelona, Spain.

[6] Departament d'Hematologia, Hospital de la Santa Creu i Sant Pau, 08025, Barcelona, Spain.

[7] Servei de Microscòpia, Universitat Autònoma de Barcelona, Bellaterra, 08193 Barcelona, Spain.

[8] Departament de Biologia Evolutiva, Ecologia i Ciències Ambientals, Facultat de Biologia, Universitat de Barcelona. 08028 Barcelona, Spain.

Keywords: scaffold proteins, self-assembling, nanoparticles, drug delivery, biomaterials.

Abstract: Self-assembling non-immunoglobulin scaffold proteins are a promising class of nanoscale carriers for drug delivery and interesting alternatives to antibody-based carriers that are not sufficiently efficient in systemic administration. To exploit their potentialities in clinics, protein scaffolds need to be further tailored to confer appropriate targeting and to overcome their potential immunogenicity, short half-life in plasma and proteolytic degradation. We have here engineered three human scaffold proteins as drug carrier nanoparticles to target the cytokine receptor CXCR4, a tumoral cell surface marker of high clinical relevance. The capability of these scaffolds for the selective delivery of *Monomethyl auristatin E* has been comparatively evaluated in a disseminated mouse model of human, $CXCR4^{+}$ acute myeloid leukemia. *Monomethyl auristatin E* is an ultra-potent anti-mitotic drug used against a range of hematological neoplasias, which because of its high toxicity is not currently administered as a free drug but as payload in antibody-drug conjugates. The protein nanoconjugates generated here offer a collective strength of simple manufacturing process, high proteolytic and structural stability and multivalent ligand receptor interactions that result in a highly efficient and selective delivery of the payload drug and in a potent anticancer effect. The approach shown here stresses this class of human scaffold proteins as promising alternatives to antibodies for targeted drug delivery in the rapidly evolving drug development landscape.

1. Introduction

Antibodies represent the major class of human protein scaffolds usable in cell-targeted drug delivery [1]. A variety of cytotoxic drugs bound to monoclonal antibodies (mAbs), single-chain variable fragments (scFv) or antigen-binding fragments (Fab) directed against cell-surface markers have been developed to generate antibody-drug conjugates (ADCs) for cancer therapy [2, 3]. In this simple coupling strategy, mAbs or Ab derivatives confer nanoscale size as well as specific cell targeting to the whole drug complex. However, the production of immunoglobulin proteins has posed many challenges due to their complex structure, low yields and expensive production cost [4]. Moreover, antibodies only confer monovalent or divalent binding to the target cells and show poor penetrability into the tumor tissue, leading to frequent life-threatening toxicities. In this context, the development of non-antibody protein scaffolds overcoming the limitations of mAbs might become of paramount significance.

Suitable scaffolds would comprise single-chain proteins with high conformational stability and convenient production yield as recombinant forms. A large number of non-antibody scaffolds are currently under active development such as affibodies, affilins, anticalins, fynomers, kunitz domains, peptide-related avimers, bicyclic peptides and cys-knots, as well as full-length proteins such as the green fluorescent protein (GFP) and thioredoxin A among others [5, 6]. Although several candidates have progressed into clinical studies showing great potential in terms of affinity, specificity and stability, only few of them have obtained regulatory approval. The main reasons for discontinuation of those attractive protein materials lie in their potential immunogenicity, very short half-life in plasma and proteolytic degradation [5, 7]. Not surprisingly, most of the protein or protein segments currently under clinical development as drug transporters are of human origin, being this feature a primary requirement for their therapeutic application [8]. Along with this, the short residence time of proteins in the bloodstream and their rapid degradation by cellular proteases impair their accumulation at a site

of pharmacological action. Consequently, most protein scaffold-based drug candidates require further engineering or a tailored presentation to increase size and minimize single-pass renal elimination [9, 10].

In this context, we have described an appealing oligomerization approach to obtain fully functional self-assembling protein-only nanostructures, based on the combination of a cationic peptide at the amino terminus of the scaffold protein along with a poly-histidine tag at the carboxy terminus [11, 12]. Such tag combination promotes the self-assembling of the fusion protein monomers in proteolytically stable multimeric nanoparticles of between 10-80 nm in size, stabilized by divalent cation coordination and non-covalent interactions [13, 14] that show high architectonic stability *in vivo* and efficiently avoid renal filtration [9]. Based on this strategy, a well-characterized protein nanoparticle (based on the self-assembling protein T22-GFP-H6) has been recently reported as a promising tumor-targeted drug vehicle for the treatment of $CXCR4^+$ colorectal cancer [15], diffuse large B-cell lymphoma [16], and acute myeloid leukemia [17]. These nanoparticles efficiently deliver cytotoxic agents into cancer cells overexpressing the cytokine receptor CXCR4, a surface marker associated with metastasis, tumor relapse and poor survival in a variety of cancer types [18, 19]. Such targeting is conferred by the high selectivity of the peptidic CXCR4 ligand T22, incorporated into the modular construct at the N-terminal position [20, 21]. However, as immunogenicity is one of the major concerns in the development of protein therapeutics, the use of the exogenous protein GFP (from the hydromedusa *Aequorea victoria*) as scaffold strongly limits its translation to clinics. Therefore, the development of scaffolds from human origin to construct equivalent protein nanoparticles would combine the precise drug delivery performance of T22 and the lack of immunogenicity and associated risks of neutralization.

Among the small molecular weight drugs used in nanoconjugates for cancer therapies, *Monomethyl auristatin E* (MMAE) is an ultra-potent antimitotic agent that inhibits cell division by blocking the polymerization of tubulin. MMAE, being 100-1000 times more potent than other used antineoplasic drugs such as Doxorubicin, is really valuable due to its ability to kill quiescent cancer cells [22], which are often resistant to conventional chemoradiotherapy and trigger disease progression and relapse. However, due to its high toxicity, it cannot be applied as a standalone drug and it is clinically used only as payload in ADCs against a range of hematological malignancies [23, 24]. Therefore, the development of new targeted protein-based human carriers seems particularly appealing for MMAE.

In this context, we have here explored the engineering, adaptation and applicability of several human proteins as protein scaffolds to generate protein nanoparticles as convenient MMAE carriers. The resulting nanoconjugates have been evaluated for the efficient delivery of MMAE in cultured cell lines and a mouse model of disseminated human $CXCR4^+$ acute myeloid leukemia. On this conceptual bases, Nidogen [25] and Stefin A-derived [26, 27] human proteins and a newly designed scaffold based on the human chorionic gonadotropin [28] have been engineered as building blocks for CXCR4-targeted nanoparticles, further conjugated with MMAE and tested regarding their global performance as drug delivery systems. The new protein-drug conjugates developed here by simple protein engineering might address unmet clinical needs in precision medicine and succeed in the rapidly evolving drug development landscape.

2. Results

Structurally different non-antibody human protein scaffolds were selected to be incorporated and tested in the oligomerization platform, namely T22-STM-H6, T22-5CTP-H6 and T22-HSNBT-H6. Three-dimensional structures and sizes of each fusion protein predicted using

Rosetta's comparative modelling [29] are shown in Figure 1. Stefin A triple mutant (STM) is a human Stefin A-derived protein engineered to lack interactivity with any other partner protein and to remain a biologically neutral scaffold, showing in its structure both α-helix and β-sheet secondary structures [27] (Figure 1A). Despite its promising structural properties, STM has not been tested yet as a scaffold nanoparticle or as a carrier for targeted drug delivery. CTP is the C-terminal peptide of the β-chain of human chorionic gonadotropin (hCG). This peptide contains four O-glycosylation sites and provides hCG with the required durability to remain in circulation during pregnancy. It has been described that fusion of this 31 amino acid β-peptide to other proteins significantly increased their *in vivo* activity due to its extensive O-linked oligosaccharides [30]. Importantly, the CTP peptide was shown to have no effect on the interaction between hCG and its receptor [28, 31]. The biologically neutral nature of this peptide encouraged us to design, for the first time, a new scaffold protein and to study its capacity as a platform for targeted drug delivery. As CTP is too short for conventional recombinant production in bacteria, we fused five tandem copies of the β-peptide to generate the protein 5CTP (Figure 1B). HSNBT is a previously engineered scaffold protein based in the β-barrel of the human Nidogen G2 domain that contains specific point mutations addressed to abort its cross-molecular interactivity to obtain a biologically neutral scaffold [25] (Figure 1C). The performance of this protein has already been tested in a targeted drug delivery platform as CXCR4-targeted T22-HSNBT-H6 fusion protein. Self-assembling T22-HSNBT-H6 nanoparticles selectively deliver the genotoxic antimetabolite oligo-5-floxuridine to $CXCR4^+$ colorectal cancer cells, showing selective and potent antitumoral effect both *in vitro* and *in vivo* [25]. However, the versatility of this protein nanoparticle to deliver cytotoxic drugs other than oligo-5-floxuridine, with different physicochemical properties and conjugation chemistry, has been never evaluated.

Once designed, T22-HSNBT-H6 and T22-STM-H6 were successfully produced in *E. coli* and T22-5CTP-H6 in HEK 293 host cells, and cleanly purified as full-length polypeptides with expected molecular masses. Interestingly, western-blot immunodetection and MALDI-TOF mass spectrometry analysis of T22-5CTP-H6 showed the typical pattern for glycosylated proteins, being 5CTP a disordered glycoprotein with 20 glycosylation sites visualized by a complex microheterogeneity (Figure 1D).

Then, we tested the ability of fusion proteins to organize into nanostructures and to bind and penetrate $CXCR4^+$ cervical cancer cells in a receptor-dependent way. FESEM examinations of protein materials allowed to explore the nanoscale morphometry (size and shape) of nanoparticles, that showed a sphere-like geometry (Figure 2A). Moreover, DLS measurements showed that all the modular proteins spontaneously self-assembled as regular materials of slightly different size, namely around 25 nm in the case of T22-STM-H6, 60 nm in the case of T22-5CTP-H6, and 10 nm for T22-HSNBT-H6 (Figure 2B). In all cases, multimeric, and therefore multivalent nanoparticles, were easily dis-assembled into their respective building blocks in presence of 1% SDS (Figure 2B) showing sizes compatible to protein monomers as determined in the *in silico* analysis (Figure 1A).

To allow nanoparticle visualization for *in vitro* internalization studies, T22-HSNBT-H6, T22-STM-H6 and T22-5CTP-H6 nanoparticles were labelled with ATTO488 fluorescent dye molecule. ATTO488 conjugation slightly affected nanoparticle size, being especially notable for T22-STM-H6 (Figure 2B). When exposed to cultured $CXCR4^+$ HeLa cells, these targeted nanostructures showed a concentration-dependent internalization into target cells, that was superior in the case of the STM-based construct (Figure 2C). Moreover, the inhibition of the cell uptake of all protein materials by means of a specific CXCR4 antagonist, AMD3100,

demonstrated the specificity of the internalization process through precise ligand-receptor recognition, with non-significant differences among them (Figure 2D).

After that, with the aim to analyze the performance of those nanostructured proteins as targeted drug delivery systems, MMAE nanoconjugates were developed, namely T22-HSNBT-H6-MMAE, T22-STM-H6-MMAE and T22-5CTP-H6-MMAE. Nanoconjugates were generated by covalent reaction of maleimide functionalized MMAE with solvent-exposed protein lysine (K) amines or cysteine (C) thiol groups (Figure 3A). In this sense, the number of amino acids within the scaffold proteins by which conjugation can take place are 12 K for STM, 6 K for 5CTP and 6 K and 1 C for HSNBT (Supplementary figure 1). In the case of T22, the four cysteine residues present in this peptide are known to form disulfide bridges between partner cysteines and thus, these residues would not be available for MMAE conjugation. We have also spotlighted C and K residues in 3D structural models of polypeptides for easy visualization (Figure 1). Conjugation of MMAE resulted in a Poisson drug load distribution as expected for used conjugation chemistry [32, 33] with payload amounts that correlated with the number of available lysine-amine residues in each protein scaffold (supplementary figure 2). Payload in T22-5CTP-H6-MMAE could not be properly determined as its high glycosylation pattern completely prevented proper mass spectrometry interpretation although according to its available lysine-amine residues it may contain a similar amounts of conjugated MMAE than T22-HSNBT-H6. As shown by DLS measurements, MMAE conjugation significantly influenced the size of T22-HSNBT-H6 nanoparticle (T22-HSNBT-H6-MMAE: 41 nm). However, it did not affect the nanostructure state of the other polypeptides (T22-STM-H6-MMAE: 21 nm, T22-5CTP-H6-MMAE: 61 nm). In all cases, multivalent nanoparticles and conjugates were both larger than 6-8 nm [34], the recognized cut-off size for renal filtration [35] and were again easily dis-assembled into building blocks in presence of 1% SDS (Figure 3B). Afterwards, the cytotoxicity of nanoconjugates was evaluated in two different $CXCR4^{+}$

cancer cells, including human cervix carcinoma cell line (HeLa) and human Acute Myeloid Leukemia cell line (THP-1).

Incubation of nanoconjugates in HeLa cells (n=3) resulted in an inhibition of cell viability with an IC_{50} above 0.5 µM in all cases (Figure 3C). The efficiency of cell killing was compared with previously described T22-GFP-H6-MMAE nanoconjugates. Incubation of nanoconjugates in THP-1 leukemia cells (n=3), which are more sensitive to MMAE, also resulted in a clear inhibition of cell viability in all cases, showing to be especially sensitive in front of T22-STM-H6-MMAE (IC_{50}: 0,114 µM) and T22-GFP-H6-MMAE (IC_{50}: 0,063 µM) (Figure 3B, Supplementary Figure 3), which are at the same time the ones containing the highest payload (Supplementary Figure 2). In this sense, T22-HSNBT-H6-MMAE and T22-5CTP-H6-MMAE nanoconjugates presented similar IC_{50} values than in HeLa cells (IC_{50} > 0.5 µM). Finally, unconjugated nanoparticles did not affect any of both cancer cells at the highest concentration, proving the lack of toxicity of the unloaded vehicles by their own (Figure 3D).

At this point, T22-5CTP-H6-MMAE nanoconjugates were discarded for further antitumoral effectivity studies as they not only showed low effectivity over $CXCR4^+$ target cells (IC_{50} > 0.5 µM) but they also, showed low batch-to-batch reproducibility and were difficult to fully characterize, mainly because of their high glycosylated nature. Therefore, although being a very interesting scaffold proposal, all these features would strongly prevent their future clinical development.

Then, and before moving to *in vivo* studies, we performed additional characterization of selected nanoconjugates in terms of their proteolytic stability in serum and z-potential, a parameter also related with nanoparticle stability. In this sense, all samples displayed a purity above 95% with a clear molecular weight band-shift upon MMAE conjugation as determined by SDS-PAGE (Supplementary Figure 4). All nanoparticles also, showed negative values of z-

potential with no significant differences before and after drug conjugation, at exception of T22-STM-H6-MMAE that reached slightly more negative z-potential values upon MMAE addition (Supplementary Figure 5). Finally, all nanoconjugates revealed to be proteolytically stable in human serum, showing just T22-HSNBT-H6-MMAE a slight tendency to precipitate, which was only relevant at very high incubation times (Supplementary Figure 4).

To assess the anticancer effect of selected nanoconjugates *in vivo*, a disseminated acute myeloid leukemia (AML) mouse model was used. The THP-1 leukemic cells used in this model overexpress the CXCR4 receptor [17]. They also constitutively express luciferase to allow non-invasive follow-up of the fate and dissemination of the target leukemic cells. In this regard, newly developed nanoconjugates (T22-STM-H6-MMAE, T22-HSNBT-H6-MMAE) were intravenously administered with 9 doses of 100 μg every day; a dose regime previously determined to be effective for the treatment of AML [17] . Free MMAE was not included in the study as it is to toxic to be administered as a standalone drug and can only be used as a payload of targeted nanocarriers [23, 24]. Thus, administered nanoconjugates were expected to selectively internalize into $CXCR4^+$ cancer cells and be subsequently degraded into cell lysosomes to finally release free and active MMAE into their cytoplasm to specifically exert its action in target cells. The experimental design and sample size are depicted in Figure 4A. The treatment did not alter body weight of mice during the entire period of the experiment (Figure 4B). Importantly, treatment with the nanoconjugate resulted in an efficient inhibition of AML dissemination in all cases comparing with the buffer-treated group. From day 10 and until the end of the experiment, nanoconjugate-treated groups showed a total body bioluminescence lower than that observed in the Buffer group (Figure 5). The anticancer effectiveness of the nanoconjugates was also observed *ex vivo* measuring luminescence emission by leukemic cells in AML-affected organs (liver, spleen and bone marrow). The results showed a significant decrease in the dissemination of leukemic cells to these tissues as

compared to the buffer-treated group (Figure 6). In the experiment performed, the effectiveness of these nanoconjugates was compared to an already characterized T22-GFP-H6-MMAE nanoconjugate [17]. The results revealed that newly developed humanized nanoconjugates were equally potent and offer exceptional performance *in vivo*, as seen for T22-GFP-H6-MMAE conjugates.

Finally, we carefully completed a histological observation of normal cells in non-targeted organs (lung, brain, pancreas, heart, and kidney) and did not observe any alteration in MMAE-nanoconjugate treated mice (results not shown), indicating similar lack of accumulation and toxicity over non-targeted tissues and stressing again the selectivity of T22 for binding CXCR4-overexpressing cancer cells and tissues as shown earlier [15].

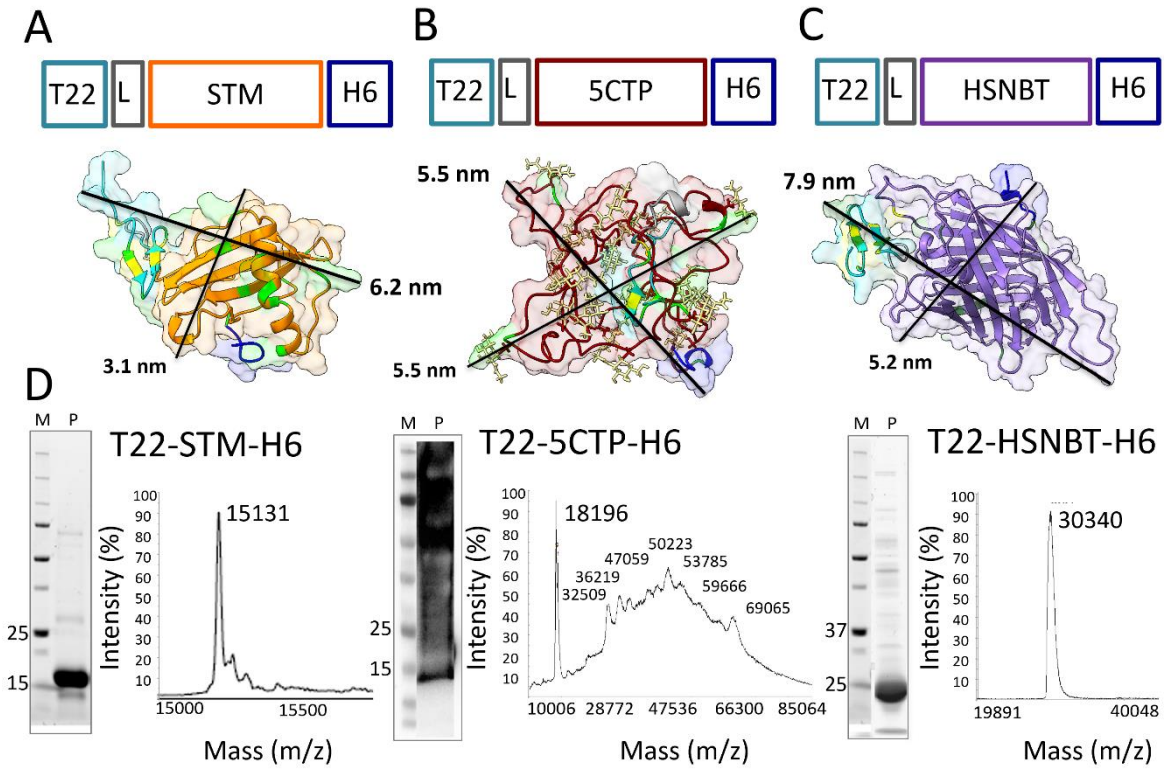

Figure 1. Modular organization and three-dimensional predicted structure of (A) T22-STM-H6, (B) T22-5CTP-H6 and (C) T22-HSNBT-H6. The N-terminal targeting peptide T22 is shown in turquoise boxes, the flexible linker (L, GGSSRSS) in grey boxes and the C-terminal hexa-histidine tag (H6) in blue boxes. The core human scaffolds are represented in orange (STM), garnet (5CTP) and purple (HSNBT) boxes. In the models, the residues critical for drug conjugation are stressed in yellow (Cys) and green (Lys). T22-5CTP-H6 contains 20 serine glycosylation sites, which are represented in the model as chemically bonded to N-acetylgalactosamine (GalNac) molecules (shown in khaki), one of the O-linked glycans present in the protein. The protein is in fact attached to different sugars resulting in a complex heterogenous glycoprotein mixture. Note that 5CTP in T22-5CTP-H6 is an intrinsically disordered region. Therefore, the structure shown here is one of the many plausible conformations. (D) Visualization by Western-blot (left) and MALDI-TOF mass spectrometry analysis (right) of purified T22-STM-H6, T22-5CTP-H6 and T22-HSNBT-H6. M and P represent the marker and protein lanes respectively. Numbers siding the marker lane indicate the molecular masses of relevant marker bands, in kDa.

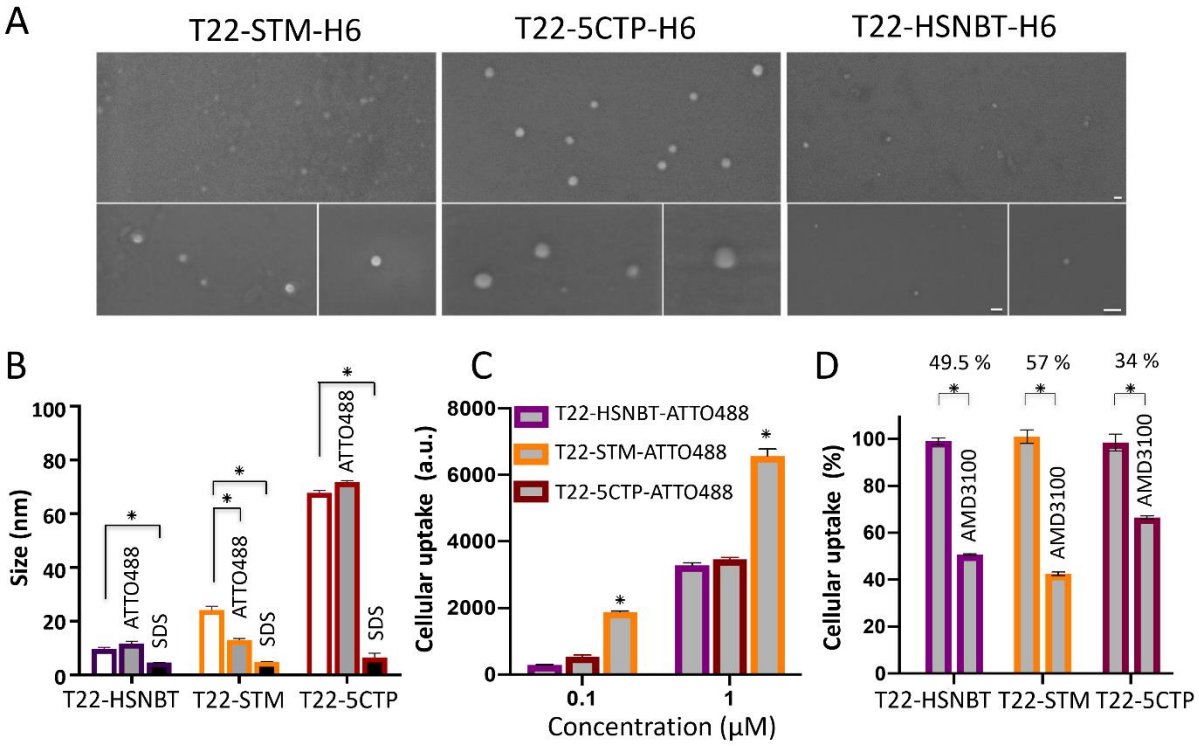

Figure 2. Characterization and cell internalization of protein nanoparticles constructed with different scaffold building blocks. For space reasons, the H6 notation has been removed from the proteins names but the tag is actually present in all the constructs. (A) Representative high-resolution images of T22-STM-H6, T22-5CTP-H6 and T22-HSNBT-H6 to show round shape and stable size of nanoconstructs. The zoom is equal in all samples, being the bars size 50 nm. (B) Hydrodynamic size distribution of nanoparticles in their native state, upon conjugation with ATTO488 (ATTO488) or upon dis-assembling with SDS (SDS). (C) Dose-dependent uptake of ATTO488-labelled T22-HSNBT-H6, T22-STM-H6 and T22-5CTP-H6 nanoparticles in $CXCR4^+$ HeLa cells upon 24 h of exposure. a.u. are arbitrary fluorescent units. (D) Inhibition of protein uptake by the CXCR4 antagonist AMD3100 upon 1 h of exposure, showing the percentage of inhibition. All data are expressed as mean ± standard error. Significant differences between relevant data pairs are indicated as * for $p < 0.01$.

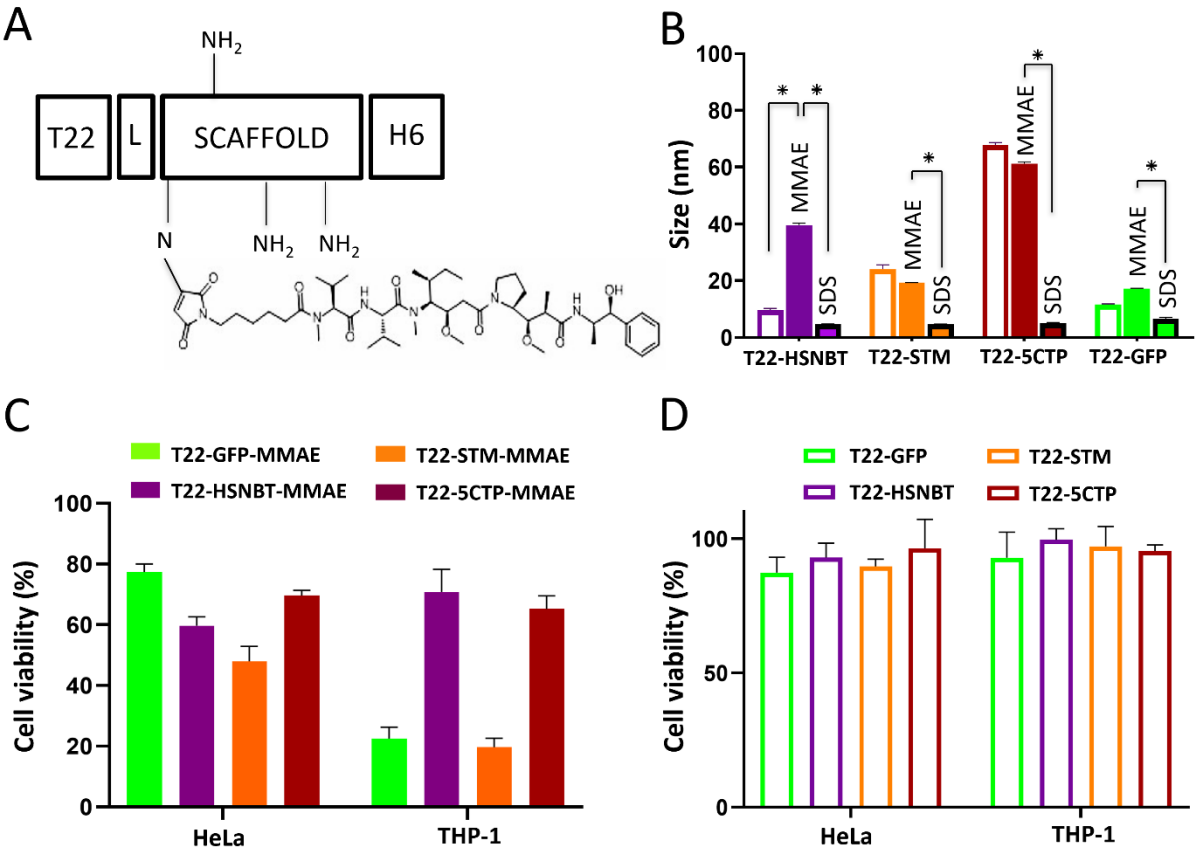

Figure 3. Generation and characterization of MMAE-protein nanoconjugates. (A) Schematic representation of the nanoconjugate based on a fusion protein T22-Scaffold protein-H6 bound to the payload drug MMAE. There is a covalent reaction of maleimide functionalized MMAE with exposed protein lysine-amine groups and cysteine-thiol groups. These residues have been also depicted in Figure 1. The number of residues in proteins scaffold that are susceptible to be conjugated with MMAE are 12 K for STM, 6 K for 5CTP and 6 K and 1 C for HSNBT. (B) Peak size distribution of MMAE-nanoconjugates in their native state (MMAE) and upon dis-assembling with SDS (SDS) measured by DLS. (C) Cell death induced by 0.5 μM of MMAE-nanoconjugates over $CXCR4^+$ HeLa and THP-1 cells upon 48 h of exposure. (D) Cytotoxicity of non-conjugated nanoparticles in $CXCR4^+$ HeLa and THP-1 cells at 2 μM during 48 h of exposure. Previously described T22-GFP-H6-MMAE nanoconjugates have been included as a control in all experiments. H6 has been removed from the names for clarity. Significant differences between relevant data pairs are indicated as * for $p < 0.01$. All data are presented as mean ± SE (n = 3).

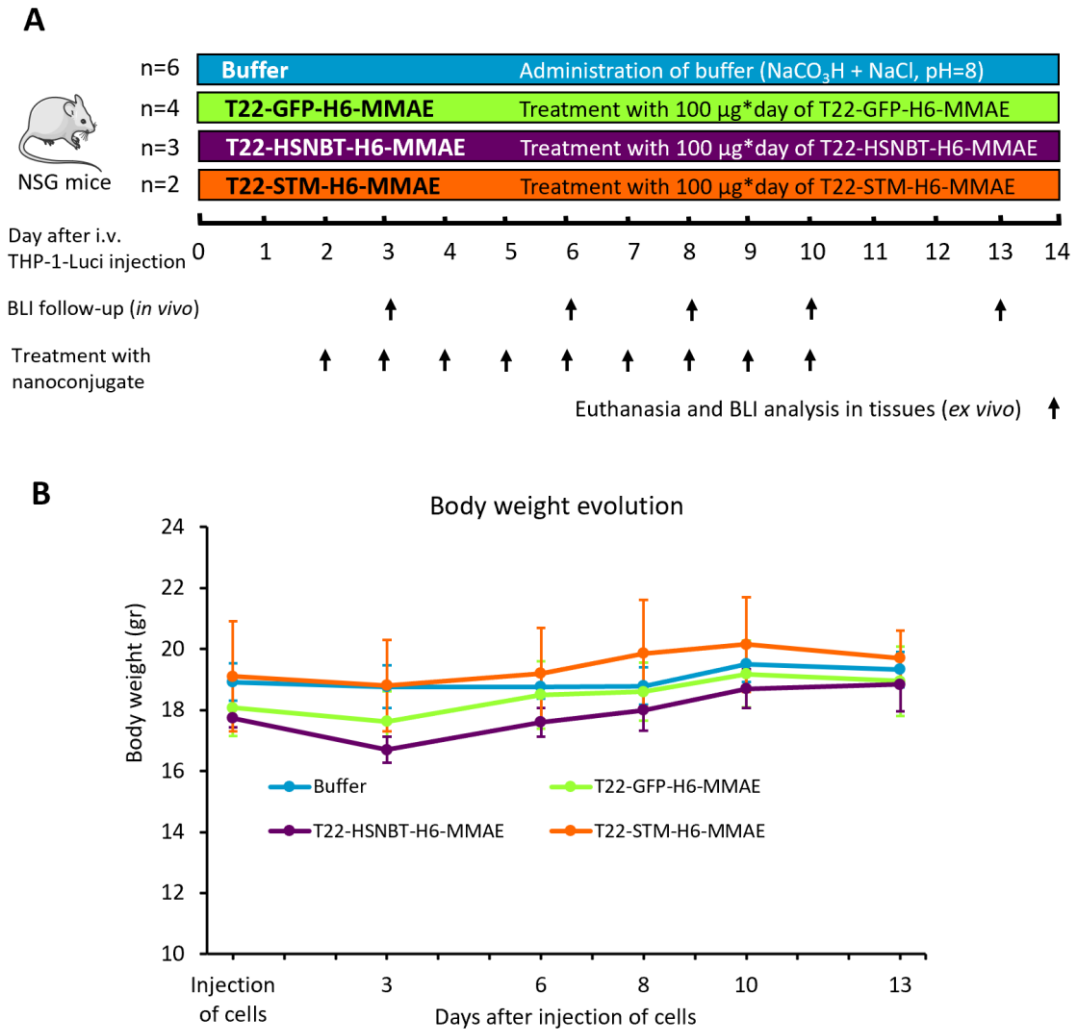

Figure 4. (A) Experimental design used to evaluate the antineoplastic activity of the different nanoparticles in a disseminated AML mouse model. (B) Measurement of total body weight of mice during the experiment according to the treatment. i.v. is intravenous injection.

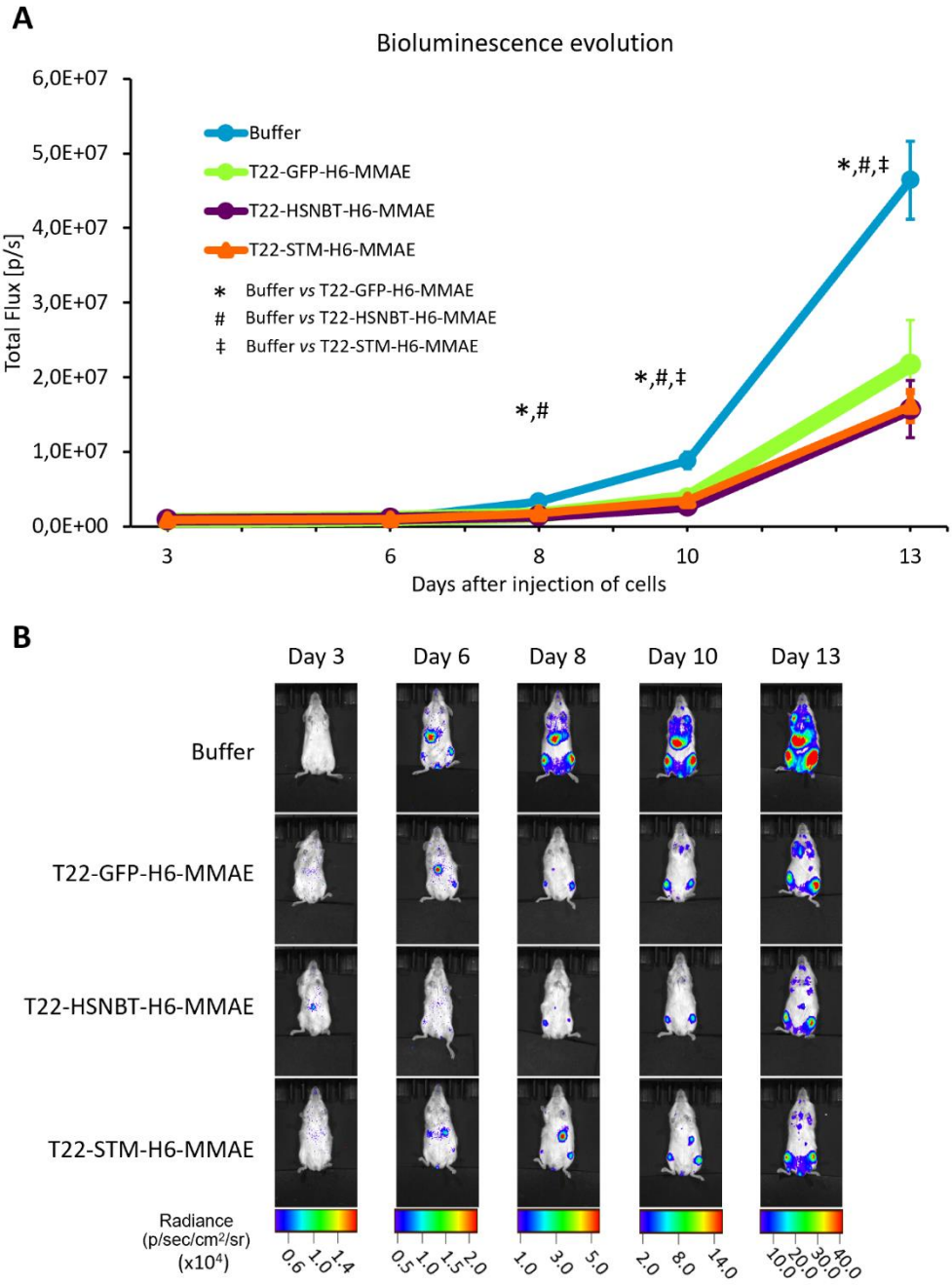

Figure 5. (A) Comparison of BLI evolution measured in IVIS Spectrum in mice treated with buffer or the nanoconjugates with different scaffolds, 3, 6, 8, 10 and 13 days after injection of THP-1-Luci cells. Results are presented as the mean of BLI total flux [photons/second] ± SE. *, # and ‡ labels significant pairwise differences ($p < 0.05$) between the buffer-treated group and the T22-GFP-H6-MMAE, T22-HSNBT-H6-MMAE, T22-STM-H6-MMAE-treated groups, respectively. (B) Representative images of the BLI follow-up of mice according to the treatment monitored in IVIS Spectrum during the experiment. BLI; bioluminescence. SE; standard error.

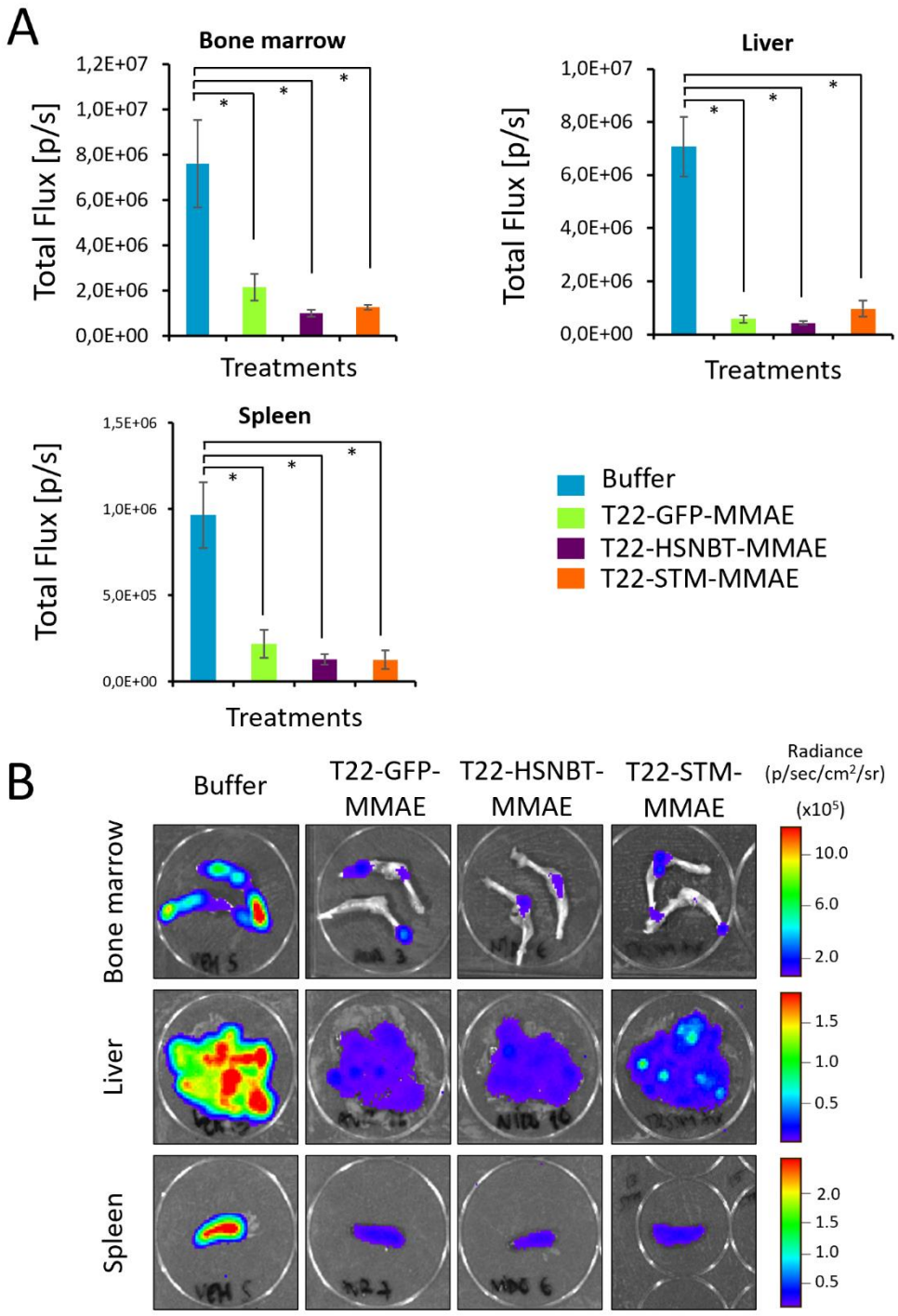

Figure 6. (A) *Ex vivo* quantification of bioluminescence (BLI) in bone marrow, liver and spleen measured in IVIS Spectrum according to the treatment after euthanasia of mice. Results are presented as the mean of BLI total flux [photons/second] ± SE and * labels significant pairwise differences ($p < 0.05$) between groups. (B) Representative images of bone marrow, liver and spleen showing BLI of tissues (radiance) at the final of the experiment according to the treatment analyzed in IVIS Spectrum. SE; standard error.

3. Discussion

Currently, molecular therapies of cancer are mainly based on unspecific cytotoxic drugs, most of them being small molecular weight chemicals that are administered systemically in the complete absence of targeting. Unfortunately, the therapeutic use of conventional cancer treatments is stalling due to drug resistance and lack of tumor and cell selectivity [36, 37]. In this context, proteins are a promising approach for the development of anticancer agents for precision medicine since they provide high versatility, biocompatibility, biodegradability, and upon conjugation with ligands, promote active targeting of cancer cells by binding to overexpressed cell-surface receptors.[8] While the first approved cancer biologics were monoclonal antibodies, emerging protein therapeutics under development are single-chain proteins that contain combinatorial or rational engineering together with tailored modifications and novel protein architectures [5]. In this sense, recombinant DNA technologies allow single-chain proteins to be empowered with accessory domains for oligomerization and targeting. These agents provide half-life extension, enhance stability and exploit multivalency to increase target selectivity [9].

Antibodies that direct MMAE to specific cancer cells are attractive protein drugs currently under development against a range of lymphomas, leukemias and solid tumors. This approach involves the FDA approved brentuximab vedotin as a treatment for patients with primary cutaneous anaplastic large cell lymphoma (pcALCL) [38] and Hodgkin lymphoma (HL) [39] and also, the recently approved polatuzumab vedotin (United States in 2019 and Europe in 2020) and enfortumab vedotin (United States in 2019) for the treatment of diffuse large B-cell lymphoma (DLBCL) [40, 41] and metastatic urothelial cancer [42], respectively. However, MMAE-mAbs show severe side effects such as peripheral neuropathy and neutropenia and also, some of them display low clinical effectiveness [43]. As MMAE is a valuable agent against a

variety of tumors, these evidences clearly reinforce the urgent need to develop new targeted protein vehicles for this drug without negative effects.

Here, we have used the previously characterized human scaffold proteins STM and HSNBT along with a totally new protein scaffold derived from human chorionic gonadotropin, 5CTP (Figure 1). These proteins, fused to the peptide T22 at their amino terminus and a poly-histidine tag H6 at their carboxy terminus, spontaneously self-assembled into CXCR4-targeted multimeric nanoparticles, with size distributions larger than 6-8 nm, the size cut-off for renal filtration (Figure 2), which is important to prolong their circulation time. Upon conjugation with MMAE, we observed CXCR4-dependent internalization and killing of $CXCR4^+$ cancer cells for all nanoconjugates *in vitro* (Figure 2, 3), being T22-5CTP-H6-MMAE the only one showing some characterization and batch-to-batch reproducibility problems. More importantly, we report a potent antineoplastic effect for selected T22-STM-H6-MMAE and T22-HSNBT-H6-MMAE nanoconjugates *in vivo* and a decrease of leukemic cell dissemination in the absence of toxicity in non-targeted tissues (Figure 5, 6), upon systemic administration. Therefore, we present these protein nanoparticle scaffolds as especially valuable therapeutics, being alternative to antibodies for targeted drug delivery for various reasons.

This is because of the highly efficient delivery of the payload drug supported by the design of a targeted nanoparticle that shows long-lasting systemic circulation by avoiding renal filtration and importantly, the multivalent display of a genetically fused specific ligand that binds the CXCR4 tumoral marker [44]. As antibodies only confer monovalent or divalent binding to the target cells, they frequently show poor biodistribution and penetrability into target cells [45]. However, the multivalent presentation of targeting ligand in these nanoparticles, achieved by the spontaneous oligomerization of protein monomers, fully exploits the high overexpression level of CXCR4 in cancer cells as compared to normal cells [46]. It must be noted that receptor-

mediated internalization of targeted nanomaterials and drugs is not linearly dependent of the concentration of the receptor, but mostly based on a threshold level that triggers a cooperative ligand binding and allowing an efficient internalization [47]. T22-empowered nanoparticles provide an efficient drug internalization into $CXCR4^{+}$ cells that is essential for antitumor activity [48]. In this context, ADCs reach only 0.01-0.1 % of the injected dose in cancer cells leading to severe adverse drug reactions [49]. In contrast, we have reported that T22-GFP-H6 nanoparticles and the derivate nanoconjugates could achieve around 85 % of the administered dose in tumor tissues, improving notably the biodistribution of ADCs without having an impact on normal cells [15, 16].

Also, antibodies are not biologically inert, since in addition to their antigen-specific Fab region, that provides targeting when used as a scaffold, their Fc fragment displays effector functions [50]. Engagement of these functions could kill off-target cells that express Fc receptors, leading to severe off-target toxicities of ADCs, that are especially severe in bi-specific ADCs. This fact lowers their therapeutic window [51]. Finally, the immune responses to therapeutic proteins such as ADCs have always been of very high concern. The approved MMAE-mAbs are chimeric molecules or humanized proteins that show an important immunogenic potential [7, 43]. Here, we have explored scaffold proteins from human origin that might be less immunogenic right from the start. Besides this, mAb-based therapeutics are associated with extremely high cost of production that limit their development at large scale [52]. For instance, the Australian Pharmaceutical Benefits Advisory Committee claimed that on the basis of inadequate cost-benefit, brentuximab vedotin would not be made available for first-line treatment [53]. mAbs are too big to be synthesized chemically and too complex to be produced in microorganisms as recombinant versions. However, customized solutions for the cost-effective production of recombinant proteins in microbial expression systems have been

developed which may enable a simple manufacturing process of the recombinant protein nanoparticles described here [54].

4. Conclusion

Engineered human non-antibody protein scaffolds have been a hot topic in the last few years, becoming invaluable tools for the design of innovative protein drugs in biotechnological and pharmaceutical applications. The nanostructured protein scaffolds developed here, show architectonic stability, multivalent display of the targeting ligand, intracellular accumulation in $CXCR4^+$ target cells and efficient delivery of MMAE drug to leukemic cells in an AML mouse model, resulting in potent antineoplastic activity. Only the highly glycosylated protein scaffold have showed some considerable limitations for its pharmaceutical application. Thus, the robust stability and efficient functionality of tested proteins in the receptor-mediated intracellular delivery of cytotoxic drugs may allow adapting these promising types of non-glycosylated human proteins into validated therapeutic modalities for precision medicines based on selective targeting.

5. Experimental Section/Methods

In silico protein modelling and visualization:

Rosetta comparative modelling approach was used through the Robetta web server (http://robetta.barkerlab.org) to predict three-dimensional models of T22-STM-H6 and T22-HSNBT-H6. In both cases, parameters were set to 10 sampling models, 1 register shift and a probability of 0.1 of sampling fragments within template regions. For T22-STM-H6, the solved structure of human cystatin A (PDB ID 1GD3, residues 1-98) was used as a template. Regarding T22-HSNBT-H6, the chosen template was the G2 domain of mouse Nidogen-1 (PDB ID 1H4U, residues 400-631) because it is the closest 3D structure available and has a high sequence

similarity with the human version. In turn, the *Ab initio* Rosetta fragment assembly method was chosen in the Robetta platform to predict the three-dimensional model of T22-5CTP-H6, as the scaffold used herein has no reported structure available. For all three models, secondary structure of residues 8-10 and 13-15 (from T22) was restricted to a beta sheet, based on previous knowledge. After the modelling process, candidates with the lowest error estimate were selected. The representation of three-dimensional structures was performed with Chimera X software (v 1.2.5) [55].

Protein production:

T22-HSNBT-H6, T22-STM-H6 and T22-5CTP-H6 proteins were designed in house and synthesized by Geneart (Thermo Fisher). T22-HSNBT-H6 and T22-STM-H6 were subcloned into pET22b plasmid (Novagen) and T22-5CTP-H6 into pTriEX-6 plasmid (Novagen). Plasmids encode genes with optimized codon usage for production host. For T22-HSNBT-H6 and T22-STM-H6 production, *E. coli* Origami B strain (Novagen) was transformed by heat shock with pET22b plasmids and cultured in Lysogeny broth medium (Sigma-Aldrich) for protein production at 37 ºC and 250 rpm, growing up to 0.5 OD_{550} units. Gene expression was induced with 0.1 mM isopropil-β-D-1-tiogalactopyranoside (IPTG) and cultures were incubated over-night at 20 ºC and 250 rpm. Cells were then harvested by centrifugation (10 min at 5,000 *g*) and resuspended in wash buffer (20 mM Tris, 500 mM NaCl, 10 mM Imidazole; pH 8) containing an EDTA-free protease inhibitor cocktail (Roche). Afterward, *E. coli* cells were disrupted by pressuring at 1200 psi by 3 rounds in a French Press (Thermo Fisher) and soluble fraction of cells obtained by centrifugation (45 min at 15,000 *g*).

For T22-5CTP-H6 production, the *E. coli* strain DH5a was used for plasmid amplification. The vector was purified from the corresponding overnight DH5a cultures, using the EndoFree Plasmid Maxi Kit (Qiagen). Absorbances at 260 nm (A260) and 280 nm (A280) were measured to quantify the plasmid and only the preparations with A260/A280 ratio higher than 1.75 were

used for the production. The FreeStyleTM HEK 293-F cell line was used to produce T22-5CTP-H6. This cell line was cultured in the serum-free FreeStyleTM 293 expression medium (Gibco) and maintained at 37 ºC on an orbital shaker platform, at 120 rpm and 8 % CO_2. HEK 293F cells were seeded at $5 \cdot 10^5$ cells/mL in a 1000-mL shaker flask containing FreeStyleTM 293 expression medium. The next day, cells were checked to be at 10^6 cells/mL and transfected with the pTriEX-6 plasmid containing the gene for T22-5CTP-H6 (1 µg plasmid DNA/mL culture and a ratio DNA:polyethylenimine of 1:3). It was further incubated during 7 days in agitation (120 rpm) at 37 ºC in 8 % CO_2. The designed protein contains a signal peptide that promotes the secretion of the T22-5CTP-H6 into culture medium. Thus, clarified supernatant of transfected culture was obtained by centrifugation (15 min at 300 g) and further filtration with 0.22 µm filters.

Protein purification:

Produced proteins were purified by His-tag affinity chromatography using 1 mL HisTrap HP column (GE Healthcare) for T22-HSNBT-H6 and T22-STM-H6 and 1 mL HisTrap excel column (GE Healthcare) for T22-5CTP-H6 through an ÄKTA pure system (GE Healthcare). Protein separations were made by linear gradient of elution buffer (20 mM Tris, 500 mM NaCl and 500 mM imidazole; pH 8). Purified protein fractions were then dialyzed against sodium carbonate buffer (166 mM $NaCO_3H$; pH 8). Protein purity was analyzed by conventional denaturing SDS-polyacrylamide gel electrophoresis and subsequent Western-blot immunodetection using anti-His monoclonal antibody (Santa Cruz Biotechnology). Finally, protein integrity and glycosylation were determined by MALDI-TOF mass spectrometry.

Morphometric characterization:

Volume size distribution of produced self-assembling protein nanoparticles was determined by Dynamic Light Scattering (DLS) at 633 nm in a Zetasizer Nano ZS (Malvern Instruments). For

that, 50 µL of each sample in sodium carbonate buffer were measured in triplicate (n=3) and the average size expressed as mean ± standard error. Protein building block were measured in triplicate (n=3) after nanoparticles dis-assembling in presence of 1 % Sodium Dodecyl Sulfate (SDS).

High-resolution electron microscopy imaging of T22-HSNBT-H6, T22-STM-H6 and T22-5CTP-H6 nanoparticles was performed. Drops of 5 µL of NPs resuspended in its buffer were directly deposited on silicon wafers (Ted Pella Inc.) for 1 min, excess of liquid blotted, air dried, and immediately observed without coating at nearly native state in a field emission scanning electron microscope (FESEM) Merlin (Zeiss) operating at 0.8 kV and equipped with an *in lens* secondary electron detector. Representative images from general fields to nanostructure details were captured at three high magnifications (200,000x, 400,000x, and 600,000x).

Zeta potential:

Z potential of protein nanoparticles and nanoconjugates were measured in triplicate (n=3) by Electrophoretic Light Scattering (ELS) in a Zetasizer Advanced Pro Blue (Malvern Instruments Limited) at 25 ºC in sodium carbonate buffer (166mM $NaHCO_3$, pH 8.0).

Cellular uptake:

Proteins were labelled with a fluorescent dye to track the internalization of nanoparticles when performing *in vitro* experiments. Briefly, T22-HSNBT-H6, T22-5CTP-H6 and T22-STM-H6 were labelled with ATTO488 (Sigma-Aldrich) through solvent-exposed lysine amines. For that purpose, protein nanoparticles and ATTO488-NHS ester molecules were incubated (1:2 molar ratio) in sodium carbonate buffer at room temperature in darkness. After 1 h of incubation, the reaction mixture was centrifuged at 4 ºC (15 min at 15,000 *g*) and dialyzed overnight in carbonate buffer to remove non-reacted free ATTO488.

Protein internalization was analyzed in $CXCR4^+$ HeLa cell (ATCC, CCL-2) cultured in 24-well plates at $3 \cdot 10^4$ cells/well by flow cytometry. Cells were cultured in MEM alpha medium supplemented with 10 % of fetal bovine serum (FBS, Gibco) in humidified atmosphere and 5 % CO_2 at 37 ºC until reaching 70 % of cell confluence. Then, upon medium removal, cells were washed in PBS and culture medium substituted by a serum-free Optipro medium (Thermo Fisher). Afterwards, 0.1 and 1 µM of ATTO488 labelled nanoparticles were added and incubated for 1 h to allow cell binding and internalization. For competition assay, HeLa cells were incubated with the CXCR4 receptor antagonist AMD3100 (octahydrochloride hydrate, Sigma-Aldrich) 1 h before protein addition, which is expected to inhibit the interaction with T22. Then, 0.1 µM of nanoparticles were added during 1 h. After protein exposure, cells were detached using 1 mg/mL Trypsin-EDTA (Gibco) for 15 min at 37 ºC, a "harsh" trypsin digestion to remove externally attached protein. The internalization was analyzed by a FACS-Canto flow cytometer (Becton Dickinson) using a 15 mW air-cooled argon ion laser at 488 nm excitation. Experiments were performed in duplicate. For comparative analyses, the intensity of fluorescence was corrected by protein amounts to render specific emission values.

Development of MMAE nanoconjugates:

Monomethyl Auristatin E (MMAE) was obtained by custom synthesis (Levena Biopharma) as a maleimide functionalized MMAE (MC-MMAE). T22-HSNBT-H6, T22-STM-H6 and T22-5CTP-H6 protein nanoparticles were covalently linked to the therapeutic moiety (MC-MMAE) through external protein Cys-Thiol and Lys-amines. For that, an excess of MC-MMAE was incubated with nanoparticles in a 1:10 ratio (protein:MC-MMAE) for T22-HSNBT-H6 and in a 1:50 ratio for T22-STM-H6 and T22-5CTP-H6 during 4 h at room temperature. In order to remove non-reacted free MC-MMAE, resulting nanoconjugates where then again purified by

IMAC affinity chromatography using HisTrap HP 1 mL columns in an ÄKTA pure (GE Healthcare) and dialyzed against original buffer (166 mM $NaCO_3H$; pH8).

***In vitro* cytotoxicity:**

HeLa cells (ATCC, CCL-2) were incubated in opaque 96-well plates in 90 µl of MEM alpha medium (Gibco) containing 10 % of Fetal bovine serum (Gibco) in humidified atmosphere and 5 % CO 2 at 37 ºC until reaching 70% confluence. MMAE-nanoconjugates were added at 0.5 µM and incubated for 48 h. Non-conjugated nanoparticles were also added at high concentration, 2 µM during 48 h. Cell viability was then tested by CellTiter-Glo®Luminescent Cell Viability Assay (Promega) in a Victor 3 luminescent plate reader (Perkin Elmer).

THP-1 cells (Leibniz Institute DSMZ, ACC16) were cultured in RPMI-1640 medium supplemented with 10% FBS, 10mmol/L L-glutamine, 100 U/mL penicillin and 10 mg/mL streptomycin and were kept at 37 ◦C in a humidified atmosphere of 5% CO2. Cells were cultured at 2.5 × 105 cells/mL for 24 h in 96-well plates. Then, MMAE-nanoconjugates were added at selected concentrations, or their corresponding buffer, for 48h. Non-conjugated nanoparticles were also added at 2 µM during 48 h. Cells were incubated for 4h with XTT reagents (Cell Proliferation Kit II, Roche Diagnostics, Basel, Switzerland) and cell viability was quantified by measuring the absorbance at 492 nm in a FLUOstar OPTIMA spectrophotometer (BMG Labtech, Ortenberg, Germany)

All experiments were performed in triplicate and data expressed as mean percentage of viability (related to control cells) ± standard error. IC50 of different protein nanoconjugates were determined from a inhibition dose- response curve fitting using GraphPad Prism 8 software.

Stability in serum

T22-STM-H6-MMAE, T22-HSNBT-H6-MMAE and T22-GFP-H6-MMAE nanoconjugates were incubated in front of human serum (Sigma) for different times (0, 5 and 24h) at 37ºC and a final concentration of 0.5 mg/ml. Samples were then centrifuged (10 min, 10000 g) to remove insoluble aggregates. Then, the proteolytic stability of nanoconjugates was determined by loading 1 µg into a TGX stain-free SDS-PAGE gel (Bio-Rad). The same amount of serum and nanoconjugates were also separately loaded as a control.

Cells for *in vivo* study:

The luminescent THP-1-Luci cells used in the *in vivo* study are $CXCR4^+$ AML human cells (ACC-16, DSMZ) transfected with a plasmid encoding the luciferase gene that confers them bioluminescence (BLI). In brief, THP-1 cells were transfected with the pPK-CMV-F3 Fusion Vector (PromoCell GmbH) and the Lipofectamine LTX and PLUS reagents (A12621, Invitrogen, TFS) according to the manufacturer's instructions. THP-1-Luci cells were cultured in RPMI-1640 medium supplemented with 20 % FBS, 10 mmol/L L-glutamine (TFS, Gibco) and 1.5 mg/mL Geneticin for selection. Cells were kept at 37 °C in a humidified atmosphere of 5 % CO_2.

Evaluation of the antineoplastic activity of the nanoparticles in a disseminated $CXCR4^+$ AML mouse model:

All procedures with mice were conducted in accordance with the guidelines approved by the institutional animal Ethics Committee of Hospital Sant Pau. NSG (NOD-*scid* IL2Rgamma^{null}) female mice (4-week-old) were obtained from Charles River Laboratories (France). Mice were housed in microisolator units with sterile food and water *ad libitum* and maintained in specific pathogen-free (SPF) environment. After 1 week in quarantine, NSG mice were intravenously (IV) injected with $1 \cdot 10^6$ THP-1-Luci cells (in 200 µL of physiological serum) to generate the

disseminated AML mouse model. Mice were divided randomly into five different experimental groups. Two days later, one group (Buffer; n=6) was IV injected with the buffer of the nanoconjugates (166 mM $NaCO_3H$, pH 8); other group with 100 µg of T22-GFP-H6-MMAE (n=4); another group with 100 µg of T22-HSNBT-H6-MMAE (n=3) and finally another group with was IV injected with 100 µg of T22-STM-H6-MMAE (n=2). Each group was treated with a total of 9 doses administered daily until the day 10. AML dissemination in mice was monitored using the IVIS Spectrum equipment (Perkin Elmer) and animal weight was measured the same day as that of BLI analysis. All mice were euthanized the day that the first animal presented relevant signs of disease such as 10 % weight loss or lack of mobility. When that point arrived, all mice were intraperitoneally injected with luciferin and after 5 min were killed by cervical dislocation. Hindlimbs, liver and spleen were excised to analyze the BLI levels *ex vivo*. Bioluminescence measurements were expressed as Total flux of BLI (photons/second; radiance) ± standard error in both *in vivo* and *ex vivo* studies.

Statistical analysis:

Quantitative values were expressed as mean ± standard error ($\overline{x} \pm SE$) of the mean. Data were transformed when necessary and checked for normality and homogeneity of variances with Shapiro–Wilk and Levene tests, respectively. For *in vitro* experiments, pairwise divergences of nanoparticle size and internalization were evaluated using Student's t-tests. For *in vivo* and *ex vivo* assays, statistical analyses were performed in the IBM SPSS Statistics (Release 25.0, New York, NY, USA). Mann-Whitney U test was used to assess the differences between nanoparticle-treated groups with a sample size ≥ 2 and the buffer-treated group. Any differences were considered statistically significant at $p < 0.05$.

Acknowledgements

We are indebted to Agencia Estatal de Investigación (AEI) and to Fondo Europeo de Desarrollo Regional (FEDER) (grant PID2019-105416RB-I00/AEI/10.13039/501100011033 to EV and grant BIO2016-76063-R to AV), AGAUR (2017SGR-229 to AV, 2017SGR-1395 to JS and 2017SGR-865 to RM), Instituto de Salud Carlos III (grant PI18/00650 to RM and grant PI20/00400 to UU) co-funded by FEDER (A way to make Europe), the Marató de TV3 Foundation (grant 201941-30-31-32 to JS and AV), CDTI (RTC-2017-6125-1) to AV and RM and CIBER-BBN (project NANOPROTHER to AV, NANOREMOTE to EV, 4NanoMets to RM and NANOLINK to UU). We are also indebted to the Networking Research Center on Bioengineering, Biomaterials and Nanomedicine (CIBER-BBN) financed by the Instituto de Salud Carlos III, with assistance from the European Regional Development Fund. We also appreciate the Servei de Microscopia from UAB for their excellent microscopy service. Protein production and nanoparticle size characterization have been partially performed by the ICTS "NANBIOSIS", more specifically by the Protein Production Platform and by the Biomaterial Processing and Biostructuring Unit of CIBER in Bioengineering, Biomaterials & Nanomedicine (CIBER-BBN)/ IBB, at the UAB sePBioEs scientific-technical service (http://www.nanbiosis.es/portfolio/u1-protein-production-platform-ppp/). The *in vivo* work was performed by the Nanotoxicology Unit of the ICTS NANBIOSIS and the CIBER-BBN (http://www.nanbiosis.es/portfolio/u18-nanotoxicology-unit/). We are also indebted to Servei de Cultius Cel·lulars i Anticossos (SCAC) from UAB for their cell culture and flow cytometry facilities. MALDI-TOF experiments were performed at Unitat d'Espectrometria de Masses de Caracterització Molecular CCiTUB in the UB. Molecular graphics and analyses were performed with UCSF Chimera, developed by the Resource for Biocomputing, Visualization, and Informatics at the University of California, San Francisco, with support from NIH P41-GM103311. NSR was supported by a pre-doctoral fellowship from the Government of Navarra, EVD by a predoctoral fellowship from Ministerio de Ciencia, Innovación y Universidades

(FPU18/04615), UU is supported by Miguel Servet contract (CP19/00028) from ISCIII co-funded by European Social Fund (ESF investing in your future). LAC was supported by the Spanish Cancer Association (AECC) and AV received an ICREA ACADEMIA award.

Received: ((will be filled in by the editorial staff))
Revised: ((will be filled in by the editorial staff))
Published online: ((will be filled in by the editorial staff))

References

1. Kaplon, H.; Muralidharan, M.; Schneider, Z.; Reichert, J. M., *MAbs* **2020,** *12* (1), 1703531. DOI 10.1080/19420862.2019.1703531.

2. Nasiri, H.; Valedkarimi, Z.; Aghebati-Maleki, L.; Majidi, J., *J Cell Physiol* **2018,** *233* (9), 6441-6457. DOI 10.1002/jcp.26435.

3. Abdollahpour-Alitappeh, M.; Lotfinia, M.; Gharibi, T.; Mardaneh, J.; Farhadihosseinabadi, B.; Larki, P.; Faghfourian, B.; Sepehr, K. S.; Abbaszadeh-Goudarzi, K.; Abbaszadeh-Goudarzi, G.; Johari, B.; Zali, M. R.; Bagheri, N., *J Cell Physiol* **2019,** *234* (5), 5628-5642. DOI 10.1002/jcp.27419.

4. Criscitiello, C.; Morganti, S.; Curigliano, G., *Journal of hematology & oncology* **2021,** *14* (1), 20. DOI 10.1186/s13045-021-01035-z.

5. Simeon, R.; Chen, Z., *Protein Cell* **2018,** *9* (1), 3-14. DOI 10.1007/s13238-017-0386-6.

6. Vazquez-Lombardi, R.; Phan, T. G.; Zimmermann, C.; Lowe, D.; Jermutus, L.; Christ, D., *Drug Discov Today* **2015,** *20* (10), 1271-83. DOI 10.1016/j.drudis.2015.09.004.

7. Baker, M. P.; Reynolds, H. M.; Lumicisi, B.; Bryson, C. J., *Self Nonself* **2010,** *1* (4), 314-322. DOI 10.4161/self.1.4.13904.

8. Serna, N.; Sanchez-Garcia, L.; Unzueta, U.; Diaz, R.; Vazquez, E.; Mangues, R.; Villaverde, A., *Trends Biotechnol* **2017**. DOI 10.1016/j.tibtech.2017.11.007.

9. Cespedes, M. V.; Unzueta, U.; Tatkiewicz, W.; Sanchez-Chardi, A.; Conchillo-Sole, O.; Alamo, P.; Xu, Z.; Casanova, I.; Corchero, J. L.; Pesarrodona, M.; Cedano, J.; Daura, X.; Ratera, I.; Veciana, J.; Ferrer-Miralles, N.; Vazquez, E.; Villaverde, A.; Mangues, R., *ACS Nano* **2014,** *8* (5), 4166-76. DOI 10.1021/nn4055732.

10. Kalyane, D.; Raval, N.; Maheshwari, R.; Tambe, V.; Kalia, K.; Tekade, R. K., *Mater Sci Eng C Mater Biol Appl* **2019,** *98*, 1252-1276. DOI 10.1016/j.msec.2019.01.066.

11. Unzueta, U.; Ferrer-Miralles, N.; Cedano, J.; Zikung, X.; Pesarrodona, M.; Saccardo, P.; Garcia-Fruitos, E.; Domingo-Espin, J.; Kumar, P.; Gupta, K. C.; Mangues, R.; Villaverde, A.; Vazquez, E., *Biomaterials* **2012,** *33* (33), 8714-22. DOI 10.1016/j.biomaterials.2012.08.033.

12. Serna, N.; Cespedes, M. V.; Saccardo, P.; Xu, Z.; Unzueta, U.; Alamo, P.; Pesarrodona, M.; Sanchez-Chardi, A.; Roldan, M.; Mangues, R.; Vazquez, E.; Villaverde, A.; Ferrer-Miralles, N., *Nanomedicine* **2016,** *12* (5), 1241-51. DOI 10.1016/j.nano.2016.01.004.

13. Lopez-Laguna, H.; Sanchez, J.; Unzueta, U.; Mangues, R.; Vazquez, E.; Villaverde, A., *Trends in biochemical sciences* **2020,** *45* (11), 992-1003. DOI 10.1016/j.tibs.2020.08.003.

14. Lopez-Laguna, H.; Unzueta, U.; Conchillo-Sole, O.; Sanchez-Chardi, A.; Pesarrodona, M.; Cano-Garrido, O.; Volta, E.; Sanchez-Garcia, L.; Serna, N.; Saccardo, P.; Mangues, R.; Villaverde, A.; Vazquez, E., *Acta biomaterialia* **2019,** *83*, 257-264. DOI 10.1016/j.actbio.2018.10.030.

15. Cespedes, M. V.; Unzueta, U.; Avino, A.; Gallardo, A.; Alamo, P.; Sala, R.; Sanchez-Chardi, A.; Casanova, I.; Mangues, M. A.; Lopez-Pousa, A.; Eritja, R.; Villaverde, A.; Vazquez, E.; Mangues, R., *EMBO Mol Med* **2018**. DOI 10.15252/emmm.201708772.

16. Falgas, A.; Pallares, V.; Unzueta, U.; Nunez, Y.; Sierra, J.; Gallardo, A.; Alba-Castellon, L.; Mangues, M. A.; Alamo, P.; Villaverde, A.; Vazquez, E.; Mangues, R.; Casanova, I., *Int J Nanomedicine* **2021,** *16*, 1869-1888. DOI 10.2147/IJN.S289733.

17. Pallares, V.; Unzueta, U.; Falgas, A.; Sanchez-Garcia, L.; Serna, N.; Gallardo, A.; Morris, G. A.; Alba-Castellon, L.; Alamo, P.; Sierra, J.; Villaverde, A.; Vazquez, E.; Casanova, I.; Mangues, R., *J Hematol Oncol* **2020,** *13* (1), 36. DOI 10.1186/s13045-020-00863-9.

18. Choi, Y. J.; Chang, W. J.; Shin, S. W.; Park, K. H.; Kim, S. T.; Kim, Y. H., *Onco Targets Ther* **2016,** *9*, 3307-12. DOI 10.2147/OTT.S104511.

19. Wang, Y.; Xie, Y.; Oupicky, D., *Curr Pharmacol Rep* **2016,** *2* (1), 1-10. DOI 10.1007/s40495-015-0044-8.

20. Serna, N.; Alamo, P.; Ramesh, P.; Vinokurova, D.; Sanchez-Garcia, L.; Unzueta, U.; Gallardo, A.; Cespedes, M. V.; Vazquez, E.; Villaverde, A.; Mangues, R.; Medema, J. P., *J Control Release* **2020,** *320*, 96-104. DOI 10.1016/j.jconrel.2020.01.019.

21. Cespedes, M. V.; Cano-Garrido, O.; Alamo, P.; Sala, R.; Gallardo, A.; Serna, N.; Falgas, A.; Volta-Duran, E.; Casanova, I.; Sanchez-Chardi, A.; Lopez-Laguna, H.; Sanchez-Garcia, L.; Sanchez, J. M.; Unzueta, U.; Vazquez, E.; Mangues, R.; Villaverde, A., *Adv Mater* **2020,** *32* (7), e1907348. DOI 10.1002/adma.201907348.

22. Bates, D.; Eastman, A., *Br J Clin Pharmacol* **2017,** *83* (2), 255-268. DOI 10.1111/bcp.13126.

23. Pfeifer, M.; Zheng, B.; Erdmann, T.; Koeppen, H.; McCord, R.; Grau, M.; Staiger, A.; Chai, A.; Sandmann, T.; Madle, H.; Dorken, B.; Chu, Y. W.; Chen, A. I.; Lebovic, D.; Salles, G. A.; Czuczman, M. S.; Palanca-Wessels, M. C.; Press, O. W.; Advani, R.; Morschhauser, F.; Cheson, B. D.; Lenz, P.; Ott, G.; Polson, A. G.; Mundt, K. E.; Lenz, G., *Leukemia* **2015,** *29* (7), 1578-86. DOI 10.1038/leu.2015.48.

24. Mendelsohn, B. A.; Barnscher, S. D.; Snyder, J. T.; An, Z.; Dodd, J. M.; Dugal-Tessier, J., *Bioconjug Chem* **2017,** *28* (2), 371-381. DOI 10.1021/acs.bioconjchem.6b00530.

25. Alamo, P.; Cedano, J.; Conchillo-Sole, O.; Cano-Garrido, O.; Alba-Castellon, L.; Serna, N.; Avino, A.; Carrasco-Diaz, L. M.; Sanchez-Chardi, A.; Martinez-Torro, C.; Gallardo, A.; Cano, M.; Eritja, R.; Villaverde, A.; Mangues, R.; Vazquez, E.; Unzueta, U., *Acta Biomater* **2021**. DOI 10.1016/j.actbio.2021.06.001.

26. Woodman, R.; Yeh, J. T.; Laurenson, S.; Ko Ferrigno, P., *J Mol Biol* **2005,** *352* (5), 1118-33. DOI 10.1016/j.jmb.2005.08.001.

27. Hoffmann, T.; Stadler, L. K.; Busby, M.; Song, Q.; Buxton, A. T.; Wagner, S. D.; Davis, J. J.; Ko Ferrigno, P., *Protein Eng Des Sel* **2010,** *23* (5), 403-13. DOI 10.1093/protein/gzq012.

28. Ceaglio, N.; Gugliotta, A.; Tardivo, M. B.; Cravero, D.; Etcheverrigaray, M.; Kratje, R.; Oggero, M., *Journal of biotechnology* **2016,** *221*, 13-24. DOI 10.1016/j.jbiotec.2016.01.018.

29. Kim, D. E.; Chivian, D.; Baker, D., *Nucleic Acids Res* **2004,** *32* (Web Server issue), W526-31. DOI 10.1093/nar/gkh468.

30. Fares, F.; Havron, A.; Fima, E., *Int J Cell Biol* **2011,** *2011*, 275063. DOI 10.1155/2011/275063.

31. Bar-Ilan, A.; Livnat, T.; Hoffmann, M.; Binder, L.; Zakar, M.; Guy, R.; Felikman, Y.; Moschcovich, L.; Shenkman, B.; Monroe, D.; Hershkovitz, O.; Kenet, G.; Hart, G., *Haemophilia* **2018,** *24* (3), 477-486. DOI 10.1111/hae.13428.

32. Kim, MT.; Chen, Y.; Marhoul, J.; Jacobson, R., *Bioconjugate Chem.* **2014,** *25* (7), 1223-1232. DOI 10.1021/bc5000109.

33. Goldmacher, VS.; Amphlett, G.; Wang, L.; Lazar, AC., Mol. Pharmaceutics **2015,** *12* (6), 1738-1744. DOI 10.1021/mp5007536.

34. Du, B. J.; Jiang, X. Y.; Das, A.; Zhou, Q. H.; Yu, M. X.; Jin, R. C.; Zheng, J., *Nat Nanotechnol* **2017,** *12* (11), 1096-+. DOI 10.1038/Nnano.2017.170.

35. Feng, B.; LaPerle, J. L.; Chang, G.; Varma, M. V., *Expert Opin Drug Metab Toxicol* **2010,** *6* (8), 939-52. DOI 10.1517/17425255.2010.482930.

36. Hoelder, S.; Clarke, P. A.; Workman, P., *Mol Oncol* **2012,** *6* (2), 155-76. DOI 10.1016/j.molonc.2012.02.004.

37. Aberger, F.; Hutterer, E.; Sternberg, C.; Del Burgo, P. J.; Hartmann, T. N., *Cell Commun Signal* **2017,** *15* (1), 8. DOI 10.1186/s12964-017-0163-4.

38. Pro, B.; Advani, R.; Brice, P.; Bartlett, N. L.; Rosenblatt, J. D.; Illidge, T.; Matous, J.; Ramchandren, R.; Fanale, M.; Connors, J. M.; Fenton, K.; Huebner, D.; Pinelli, J. M.; Kennedy, D. A.; Shustov, A., *Blood* **2017,** *130* (25), 2709-2717. DOI 10.1182/blood-2017-05-780049.

39. Connors, J. M.; Jurczak, W.; Straus, D. J.; Ansell, S. M.; Kim, W. S.; Gallamini, A.; Younes, A.; Alekseev, S.; Illes, A.; Picardi, M.; Lech-Maranda, E.; Oki, Y.; Feldman, T.; Smolewski, P.; Savage, K. J.; Bartlett, N. L.; Walewski, J.; Chen, R.; Ramchandren, R.; Zinzani, P. L.; Cunningham, D.; Rosta, A.; Josephson, N. C.; Song, E.; Sachs, J.; Liu, R.; Jolin, H. A.; Huebner, D.; Radford, J.; Group, E.-S., *The New England journal of medicine* **2018,** *378* (4), 331-344. DOI 10.1056/NEJMoa1708984.

40. Sehn, L. H.; Herrera, A. F.; Flowers, C. R.; Kamdar, M. K.; McMillan, A.; Hertzberg, M.; Assouline, S.; Kim, T. M.; Kim, W. S.; Ozcan, M.; Hirata, J.; Penuel, E.; Paulson, J. N.; Cheng, J.; Ku, G.; Matasar, M. J., *J Clin Oncol* **2020,** *38* (2), 155-165. DOI 10.1200/JCO.19.00172.

41. Deeks, E. D., *Drugs* **2019,** *79* (13), 1467-1475. DOI 10.1007/s40265-019-01175-0.

42. Hanna, K. S., *Drugs* **2020,** *80* (1), 1-7. DOI 10.1007/s40265-019-01241-7.

43. Kaplon, H.; Reichert, J. M., *MAbs* **2021,** *13* (1), 1860476. DOI 10.1080/19420862.2020.1860476.

44. Rueda, F.; Cespedes, M. V.; Conchillo-Sole, O.; Sanchez-Chardi, A.; Seras-Franzoso, J.; Cubarsi, R.; Gallardo, A.; Pesarrodona, M.; Ferrer-Miralles, N.; Daura, X.; Vazquez, E.; Garcia-Fruitos, E.; Mangues, R.; Unzueta, U.; Villaverde, A., *Adv Mater* **2015,** *27* (47), 7816-22. DOI 10.1002/adma.201503676.

45. Lambert, J. M., *Mol Pharm* **2015,** *12* (6), 1701-2. DOI 10.1021/acs.molpharmaceut.5b00302.

46. Schepers, K.; Campbell, T. B.; Passegue, E., *Cell Stem Cell* **2015,** *16* (3), 254-67. DOI 10.1016/j.stem.2015.02.014.

47. Martinez-Veracoechea, F. J.; Frenkel, D., *Proc Natl Acad Sci U S A* **2011,** *108* (27), 10963-8. DOI 10.1073/pnas.1105351108.

48. Unzueta, U.; Cespedes, M. V.; Ferrer-Miralles, N.; Casanova, I.; Cedano, J.; Corchero, J. L.; Domingo-Espin, J.; Villaverde, A.; Mangues, R.; Vazquez, E., *Int J Nanomedicine* **2012,** *7*, 4533-44. DOI 10.2147/IJN.S34450.

49. Azad, B. B.; Chatterjee, S.; Lesniak, W. G.; Lisok, A.; Pullambhatla, M.; Bhujwalla, Z. M.; Pomper, M. G.; Nimmagadda, S., *Oncotarget* **2016,** *7* (11), 12344-58. DOI 10.18632/oncotarget.7111.

50. Saunders, K. O., *Front Immunol* **2019,** *10*, 1296. DOI 10.3389/fimmu.2019.01296.

51. Labrijn, A. F.; Janmaat, M. L.; Reichert, J. M.; Parren, P., *Nat Rev Drug Discov* **2019,** *18* (8), 585-608. DOI 10.1038/s41573-019-0028-1.

52. Shukla, A. A.; Wolfe, L. S.; Mostafa, S. S.; Norman, C., *Bioeng Transl Med* **2017,** *2* (1), 58-69. DOI 10.1002/btm2.10061.

53. Macaulay, R.; Siddiqui, M. K.; Stoddart, S., *Value Health Reg Issues* **2015,** *6*, 143-149. DOI 10.1016/j.vhri.2015.03.021.

54. Sanchez-Garcia, L.; Martin, L.; Mangues, R.; Ferrer-Miralles, N.; Vazquez, E.; Villaverde, A., *Microb Cell Fact* **2016,** *15*, 33. DOI 10.1186/s12934-016-0437-3.

55. Pettersen, EF.; Goddard, TD.; Huang, CC.; Meng, EC.; Couch, GS.; Croll, TI.; Horris, JH.; Ferrin, TE., *Protein Science* **2021,** *30*, 70-82. DOI 10.1002/pro.3943.